



OPEN ACCESS

Novel human D-amino acid oxidase inhibitors stabilize an active-site lid-open conformation

Ryan T. TERRY-LORENZO*¹, Lawrence E. CHUN†, Scott P. BROWN*, Michele L. R. HEFFERNAN*, Q. Kevin FANG*, Michael A. ORSINI*, Loredano POLLEGIONI‡§, Larry W. HARDY*, Kerry L. SPEAR* and Thomas H. LARGE*

*Discovery Research Department, Sunovion Pharmaceuticals, Marlborough, MA 01752, U.S.A.

†Emerald Bio, Bainbridge Island, WA 98110, U.S.A.

‡Dipartimento di Biotecnologie e Scienze della Vita, Università degli Studi dell'Insubria, Via J. H. Dunant 3, 21100 Varese, Italy

§The Protein Factory, Politecnico di Milano, ICRM-CNR Milano and Università degli Studi dell'Insubria, Via Mancinelli 7, 20131 Milano, Italy

Synopsis

The NMDAR (*N*-methyl-D-aspartate receptor) is a central regulator of synaptic plasticity and learning and memory. hDAAO (human D-amino acid oxidase) indirectly reduces NMDAR activity by degrading the NMDAR co-agonist D-serine. Since NMDAR hypofunction is thought to be a foundational defect in schizophrenia, hDAAO inhibitors have potential as treatments for schizophrenia and other nervous system disorders. Here, we sought to identify novel chemicals that inhibit hDAAO activity. We used computational tools to design a focused, purchasable library of compounds. After screening this library for hDAAO inhibition, we identified the structurally novel compound, 'compound **2**' [3-(7-hydroxy-2-oxo-4-phenyl-2H-chromen-6-yl)propanoic acid], which displayed low nM hDAAO inhibitory potency ($K_i = 7$ nM). Although the library was expected to enrich for compounds that were competitive for both D-serine and FAD, compound **2** actually was FAD uncompetitive, much like canonical hDAAO inhibitors such as benzoic acid. Compound **2** and an analog were independently co-crystallized with hDAAO. These compounds stabilized a novel conformation of hDAAO in which the active-site lid was in an open position. These results confirm previous hypotheses regarding active-site lid flexibility of mammalian D-amino acid oxidases and could assist in the design of the next generation of hDAAO inhibitors.

Key words: crystallography, DAAO, DAO, drug discovery, NMDA receptor, schizophrenia

Cite this article as: Terry-Lorenzo, R.T., Chun, L.E., Brown, S.P., Heffernan, M.L.R., Fang, Q.K., Orsini, M.A., Pollegioni, L., Hardy, L.W., Spear, K.L. and Large, T.H. (2014) Novel human D-amino acid oxidase inhibitors stabilize an active-site lid-open conformation. *Biosci. Rep.* **34**(4), art:e00133.doi:10.1042/BSR20140071

INTRODUCTION

DAAO (D-amino acid oxidase) is a flavoprotein with exquisite stereospecificity for catalysing the oxidation and, hence, degradation of D-amino acids [1,2]. DAAO has been studied for many decades and its catalytic mechanism is well-understood. Using FAD as cofactor, DAAO binds to D-amino acids and, via a hydride transfer mechanism, oxidizes the amino acid and, in the process, reduces the FAD cofactor. DAAO has weak activity towards D-amino acids with acidic side chains, but has significant activity to oxidize a diversity of D-amino acids, typically amino acids with small hydrophilic, large aromatic or basic side chains [1,2].

DAAO is evolutionarily conserved, and in mammals, the significant levels of DAAO protein and enzymatic activity are found in the kidney, liver (some species) and brain [3]. Although the function of DAAO in liver and kidney is likely to degrade D-amino acids originating from bacterial sources [4], the function of DAAO in the mammalian brain was mysterious until the early 1990s, when it was determined that the mammalian brain contains D-amino acids, most notably D-serine [5,6]. Furthermore, brain D-serine exists at concentrations sufficient for functionally serving as a co-agonist at the glycine site of the NMDA (*N*-methyl-D-aspartate) receptor [7–9]. The NMDAR is a glutamate receptor in the brain known to play a central role in the nervous system processes such as synaptic plasticity, learning and memory and pain sensation [10]. This link between D-serine and NMDAR

Abbreviations: DAAO, D-amino acid oxidase; hDAAO, human D-amino acid oxidase; HRP, horseradish peroxidase; pdb, protein data bank; rDAAO, rat DAAO; NMDAR, *N*-methyl-D-aspartate receptor.

¹ To whom correspondence should be addressed (email Ryan.Terry-Lorenzo@sunovion.com).

function suggested that, by controlling D-serine brain levels, DAAO and serine racemase, the D-serine-synthesizing enzyme [11], are also involved in regulating the key brain functions. Despite the apparent low levels of DAAO in forebrain regions [12], pharmacological studies with DAAO inhibitors [13,14], genetic studies in DAAO knockout animals [15,16] and genetic studies with serine racemase-mutated mice [17,18] have all clearly indicated that D-serine regulatory enzymes impact NMDAR function, synaptic function and cognitive ability. Furthermore, chemical regulators of D-serine metabolism could be effective disease treatments. More specifically, as NMDAR hypofunction is a core pathway deficit in schizophrenia [19,20], DAAO inhibitors, perhaps in combination with D-serine systemic administration [21], have the potential to be effective treatments of schizophrenia via their capacity to increase D-serine in the brain and enhance NMDAR-dependent functions [13,14,22]. Moreover, although the mechanistic underpinnings of DAAO's roles in nociception are not fully understood, DAAO inhibitors have been shown to reduce pain in various rodent models of neuropathic pain [23–25].

Although multiple academic laboratories and pharmaceutical companies have designed inhibitors of hDAAO (human DAAO) [26], the known collection of potent hDAAO inhibitors is structurally rather limited. Modelled after the classic inhibitor, benzoic acid, the original pharmacophore for hDAAO inhibitors was a low molecular weight, aryl-acid compound that occupied the hDAAO active site on the *re* side of the isoalloxazine ring of FAD [27]. Further efforts revealed that bioisosteric replacement of the acid could produce compounds which were also hDAAO inhibitors with low nM potency [22]. Guided by the knowledge that the active site could accommodate D-amino acids with large aromatic side chains, such as D-tryptophan [28] and D-DOPA [29], a newer generation of hDAAO inhibitors were designed that occupy the so-called 'subpocket' of the hDAAO active site [13,30,31]. Additional plasticity in the hDAAO active site beyond the *re* side of flavin and the subpocket has yet to be explored.

hDAAO, unlike other known DAAOs, has low affinity for the FAD cofactor [32], so it likely exists as an equilibrium of FAD-bound (active)- and FAD-unbound (inactive) species in physiological environments [33]. Guided by this knowledge and by the precedented FAD-competitive DAAO inhibitors described in the literature [33–35], we sought compounds that are FAD competitive. To gain specificity for hDAAO inhibition, we sought compounds that combined elements of both the D-amino acid and the flavin portion of the FAD cofactor. Such bisubstrate analogues would be expected to compete with both D-serine and FAD and would represent compounds divergent from existing hDAAO inhibitors. We used computational tools to identify a focused library of bisubstrate analogue-like compounds and screened them for hDAAO inhibition. Serendipitously, however, we discovered a compound that did not compete with FAD, but instead occupied a novel pocket in the hDAAO active site and stabilized an hDAAO conformation with its active-site lid open. The DAAO active-site lid (amino acids 216–228) had previously been hypothesized to open up to allow for substrate access [28]. The

X-ray crystal structures described here confirm this hypothesis, extend our knowledge of DAAO active-site flexibility, and enable future opportunities for structure-guided drug design of DAAO inhibitors.

EXPERIMENTAL

Compound procurement

The compounds composing the focused library were identified using computational chemistry methods. Briefly, the eMolecules catalogue of commercially available compounds was filtered for acceptable drug-like molecular properties. After filtering, compounds were computationally scored (using both 2D and 3D methods) for their potential to occupy portions of the D-amino acid and FAD-binding pockets within hDAAO. The 1016 best scoring compounds were purchased from eMolecules for screening. Please see Supplementary Online Data (at <http://www.bioscirep.org/bsr/034/bsr034e133add.htm>) for details on library assembly and screening.

Compound **1** (4H-furo[3,2-b]pyrrole-5-carboxylic acid) was synthesized as described previously [27]. Compound **2** [3-(7-hydroxy-2-oxo-4-phenyl-2H-chromen-6-yl)propanoic acid] was purchased from eMolecules as an original compound from the focused library screen. Compound **3** [4-hydroxy-6-(2-(7-hydroxy-2-oxo-4-phenyl-2H-chromen-6-yl)ethyl)pyridazin-3(2H)-one], Compound **5** (6-(2,4-dihydroxyphenethyl)-4-hydroxypyridazin-3(2H)-one) and Compound **6** (6-(2,4-dimethoxyphenethyl)-4-hydroxypyridazin-3(2H)-one) were synthesized and characterized by NMR and MS. Synthesis and analytical details are described in the Supplementary Online Data. ADP disodium salt was purchased from Sigma-Aldrich and Compound **4** was purchased from eMolecules.

Enzymatic assays

All enzymatic assays were conducted at room temperature (23–24 °C) in 96-well plate format. Dose response data to generate IC₅₀ data were analysed via Prism (Graphpad Software) or by a script executed by Pipeline Pilot (Accelrys). In each case, data were fit to a standard, four parameter equation to determine curve top, bottom, concentration producing 50% inhibition (IC₅₀) and Hill Slope.

An Amplex Red-based assay has been utilized by others to measure hDAAO product formation and screen for hDAAO inhibitors [36]. For our assay, N-terminal hexaHis (His)-tagged hDAAO (prepared as described previously [32]), HRP (horseradish peroxidase), FAD, and compound inhibitor were incubated for 20–30 min. After that pre-incubation period, D-serine and Amplex Red were added and reaction proceeded for 1 hour. Fluorescent product, caused by hydrogen peroxide-dependent, Amplex Red oxidation during hDAAO-catalysed substrate turnover, was measured on a FlexStation II (Molecular Devices) in endpoint mode with these settings: excitation 530 nm,

emission 590 nm, cutoff 590 nm and photomultiplier tube on Low. The final concentrations for reaction components were as follows: 50 mM sodium phosphate (Sigma), pH 7.4, 0.001 % (v/v) human serum albumin (Sigma), 0.73 nM His-hDAAO (prepared as described in [32]), 4 units/ml HRP (Sigma), 450 nM FAD (Sigma), 50 μ M Amplex Red (Life Technologies), 5 mM D-serine (Alfa Aesar) and 1.5 % (w/v) DMSO. For the counter assay, hDAAO was omitted and 800 nM hydrogen peroxide (Sigma) was included. For the rDAAO (rat DAAO) assay, the protocol was identical except that hDAAO was replaced with 5 nM hexaHis-tagged rDAAO (prepared as described in [37]) and D-serine concentration was increased to 30 mM.

For the LC-MS-based hDAAO inhibition assay, his-hDAAO, FAD and compound inhibitors were incubated for 20–30 min. After that period, D-phenylglycine was added and reaction proceeded for 1 h. The final concentrations for reaction components were as follows: 50 mM ammonium bicarbonate (Sigma), pH of approximately 8.0 (not adjusted), 0.001 % (v/v) human serum albumin, 5 nM His-hDAAO, 450 nM FAD, 5 mM D-phenylglycine (Sigma) and 1 % (v/v) DMSO. Following the 1 h enzymatic reaction, an equal volume of 100 % (v/v) acetonitrile was added. Quantitation of benzylformic acid concentrations was performed using negative ion liquid chromatography/mass spectrometry/mass spectrometry (LC-MS/MS). A 2 μ l aliquot of sample was injected onto an ultra-high performance liquid chromatographic system (UPLC Waters Corp) equipped with an API 5500 QTrap mass spectrometer detector (Applied Biosystems/MDS Sciex) operated in the negative TurboIonSpray[®] mode. Instrument conditions were adjusted and optimized for benzylformic acid that was monitored using transitions from m/z 149–77. The separation of benzylformic acid from extracted matrix materials was accomplished with an overall run time of 1.5 min using a Waters Acquity BEH C-18 1.8 μ m column (50 mm \times 2.1 mm) maintained at 25 °C. The mobile phases used for elution consisted of 1.0 mM ammonium formate with 0.2 % (v/v) formic acid in water (A) and 1.0 mM ammonium formate with 0.2 % (v/v) formic acid in acetonitrile (B) at a total flow rate of 0.600 ml/min. Wash solvent 1 was 3 % formic acid in acetonitrile and wash solvent 2 was 3 % formic acid in water. Calibration standards were injected once before and once after the analysis of unknown samples to construct a standard curve. A linear weighted (1/concentration²) regression analysis of the analyte peak area ratio versus theoretical concentration was used to produce calibration curves from standards.

A jump-dilution protocol [38] was utilized to confirm reversibility of compound inhibition and to determine compound apparent dissociation rate (k_{off}). The assay mixture was similar to that described above for the Amplex Red-based assay system. For the jump-dilution assay, in 5 μ l, 15–40 nM hDAAO was incubated with inhibitor compound at a high concentration (typically 6-fold higher than the IC_{50}) in the presence of 80 μ M FAD. As all the compounds tested were FAD uncompetitive, the high [FAD] facilitated inhibitor–hDAAO complex formation. After a 30 min pre-incubation to form inhibited complexes, 195 μ l of reaction mixture was added. Compared with the standard assay, 50 mM D-serine was utilized as the hDAAO substrate. With the

40-fold dilution into high-substrate concentration, after dissociation, compound re-association with hDAAO would be unlikely and marginal, as the diluted compound concentration would be well below an effective inhibitory concentration. Immediately after adding the reaction mixture, fluorescent substrate was monitored kinetically by the FlexStation II. Data were fit using the following equation [38] in which P is the fluorescent product formed, t is the time, v_s is the final, steady-state reaction velocity, v_i is the initial reaction velocity, and k is the k_{off} :

$$[P] = v_s t + \frac{v_i - v_s}{k} (1 - e^{-kt}) \quad (1)$$

To determine inhibitor mechanism of action (D-serine- or FAD-competition), saturation experiments were performed using the Amplex Red system. Keeping D-serine or FAD constant, concentration of the other substrate was varied, and hDAAO enzymatic product was measured fluorescently as described above; these saturation tests were conducted in the presence of variable amounts of inhibitor. In these experiments, there was no pre-incubation period, such that hDAAO was exposed to D-serine, FAD and inhibitor simultaneously. The final concentrations for reaction components were as follows: 50 mM sodium phosphate, pH 7.4, 0.001 % (v/v) human serum albumin, 0.15 nM hDAAO, 4 units/ml HRP, 40 μ M FAD (constant for D-serine saturation), 50 μ M Amplex Red, 50 mM D-serine (constant for FAD saturation), and 1.5 % DMSO. After a 1 h reaction, product was measured using the FlexStation II in the endpoint mode. Data were plotted and fit with a one site, specific binding equation (Graphpad Prism):

$$y = V_{\text{max}} \times \frac{x}{K_M + x} \quad (2)$$

Equation (2) permitted a determination of V_{max} and K_M at variable inhibitor concentration for a determination of competitive, uncompetitive or non-competitive profile. For D-serine competitive inhibitors, the same data were fit using the GraphPad Prism ‘Competitive inhibition’ equation to derive a global K_i value:

$$K_{M,\text{obs}} = K_M (1 + [I]K_i) \quad (3)$$

$$y = V_{\text{max}} \times \frac{x}{K_{M,\text{obs}} + x} \quad (4)$$

Crystallization and structure determination

Full-length, untagged hDAAO protein was prepared as described previously [32]. The hDAAO preparation at 2 mg/ml was dialysed overnight at 4 °C against 50 mM sodium phosphate, pH 6.6 and 10 μ M FAD prior to crystallography. hDAAO samples were incubated overnight with 250 μ M compound **3** or 1 mM compound **2** and then subjected to crystallization trials. Crystals of the compound **3** complex were grown in sitting drops containing 0.4 μ l hDAAO + 0.4 μ l crystallant consisting of 30 % (w/v) PEG2000MME, 0.1 M potassium thiocyanate. Crystals of the compound **2** complex were grown in sitting drops containing 0.4 μ l hDAAO + 0.4 μ l crystallant consisting of 13.64 % (w/v) PEG3350, 0.1 M Tris pH 7.4, 0.15 M

potassium citrate tribasic. Crystals were harvested in 20% (v/v) ethylene glycol and flash frozen in liquid nitrogen. X-ray data for the hDAAO:FAD:compound **2** complex crystals were collected at SSRL beam line 7-1 and reduced with the XDS/XSCALE package to 2.85 Å. The CCP4 program Phaser was used for Molecular Replacement using chain A from the 3CUK structure as the search model. The model was iteratively extended in real space using Coot and refined in reciprocal space using Refmac5. The final model had $R/R_{\text{free}} = 0.24/0.29$. X-ray data for the hDAAO:FAD:compound **3** complex crystals were collected at APS beam line 21-idf and reduced with the XDS/XSCALE package to 2.4 Å. The CCP4 program Molrep was used for Molecular Replacement using chain A from the 3CUK structure as the search model. The model was iteratively extended in real space using Coot and refined in reciprocal space using Refmac5. The final model had $R/R_{\text{free}} = 0.18/0.23$.

RESULTS

Characterization of compound **2** as a novel inhibitor of hDAAO

We utilized a novel screening strategy to identify compound **2**, a potent inhibitor of hDAAO (See Supplementary Online Data; compound **2** structure in Table 1). To confirm that compound **2** was a reversible inhibitor of hDAAO, we profiled it in a series of biochemical assays, using the previously characterized hDAAO inhibitor compound **1** [22,27] as positive control. As shown in Figure 1(A), compounds **1** and **2** inhibited hDAAO activity. However, they did not display inhibition in the counter assay, verifying that these compounds did not interfere with the assay detection system non-specifically. To fully exclude fluorescence artefacts that could arise in the Amplex Red system, we developed an orthogonal assay in which the direct product of the hDAAO oxidative reaction was measured by LC-MS, when D-phenylglycine was used as substrate. In this assay, both compounds **1** and **2** were confirmed as potent hDAAO inhibitors (Figure 1B and Table 1). Both compounds inhibited rDAAO, although the compounds were less potent as inhibitors of rDAAO compared with hDAAO (Figure 1C and Table 1). Compound **1** and other hDAAO inhibitors have previously been observed to be less potent rDAAO inhibitors [22]. To confirm that the compounds were reversible, we utilized a jump-dilution assay protocol, in which the inhibited enzyme–ligand complexes were diluted to allow for kinetic measurement of inhibitor dissociation and reconstitution of enzyme activity [38]. For compound **2**, we pre-incubated in 200 nM (a concentration yielding >80% inhibition; see Figure 1A), and then after dilution the compound was at 5 nM (no significant inhibition under 50 mM D-serine recovery conditions). Reaction product was recorded immediately after dilution (Figure 1D). Under these conditions, initial velocity (V_i) was low, but over time, inhibitor dissociated and a steady-state velocity (V_s) was reached. These results were consistent with reversible inhibition [38]. The recovery time course was fit with equation (1) (the Experimental

section) to obtain an apparent rate constant for dissociation (k_{off}) as reported in Table 1.

Compound **2** had the kinetic profile of an active-site hDAAO inhibitor

As described in the Supplementary Online Data section, compound **2** was hypothesized based upon ligand-based and structure-based computer modelling to occupy both the active site of hDAAO and portions of the FAD-binding site. To experimentally determine competitive behaviour of compound **2** with both substrate (D-serine) and cofactor (FAD), we tested it in D-serine and FAD saturation experiments. To confirm that our assay was capable of reporting FAD-competitive kinetic behaviour, we profiled a series of molecules that we hypothesized would be FAD competitive. One of these compounds was ADP, a molecule identical to a substructure of FAD; the ADP portion of FAD sits deep into the hDAAO protein [39]. ADP was a low-potency hDAAO inhibitor (Table 1) that we hypothesized would displace FAD and behave kinetically as FAD-competitive. In FAD saturation experiments, ADP linearly increased hDAAO $K_{M,\text{obs}}$ for FAD with minimal effect on hDAAO V_{max} (Figure 2A, top). This result is consistent with ADP being an FAD-competitive inhibitor of hDAAO and confirms that our assay could report FAD-competitive behaviour. In reciprocal D-serine saturation experiments, ADP displayed a mixed competition profile in which it both lowered V_{max} and increased $K_{M,\text{obs}}$ (Figure 2B, top). Of note, when the active site of hDAAO is occupied by a ligand, hDAAO affinity for FAD increases [32,33]; thus, even a ‘pure’ FAD competitive inhibitor would be expected to appear partially D-serine competitive in these experiments.

In contrast to ADP, compound **1**, which occupies the hDAAO active site and is stabilized by pi (π - π)-stacking interactions with the FAD cofactor [27], dose-dependently decreased both the V_{max} and $K_{M,\text{obs}}$ for FAD (Figure 2A). This uncompetitive kinetic behaviour is consistent with compound **1** binding only to the FAD-bound, hDAAO holoenzyme [27]. In saturation experiments with D-serine, compound **1** displayed classic competitive behaviour: the value of $K_{M,\text{obs}}$ for D-serine increased linearly with increasing concentration of compound **1**, whereas V_{max} was only modestly affected (Figure 2B). In summary, in our experiments, the hDAAO active-site inhibitor compound **1** was D-serine competitive and FAD uncompetitive. For D-serine competitive compounds, kinetic equations (3) and (4) (see the Experimental section) were used to derive an inhibitory constant (K_i), as reported in Table 1. For each compound, the K_i was lower (more potent) than the IC_{50} value, which was likely owing to the variable concentrations of FAD and D-serine used in the two assay formats.

Compound **2** was tested in these assays and determined to be both FAD uncompetitive (decreased FAD $K_{M,\text{obs}}$ and V_{max} , Figure 2A) and D-serine competitive (increased hDAAO $K_{M,\text{obs}}$ for D-serine without affecting V_{max} , Figure 2B). This result demonstrated that, inconsistent with the modelling predictions, compound **2** did not compete with FAD. Rather, despite its larger molecular mass relative to previously reported active-site hDAAO

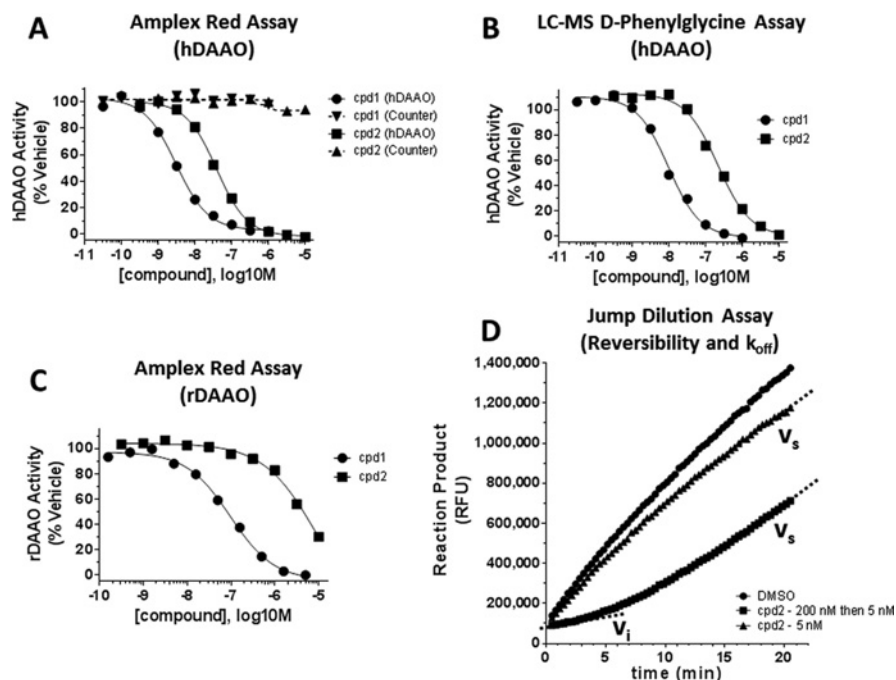


Figure 1 Profiling compounds in enzymatic inhibitory assays

(A) In the Amplex Red platform, compound (cpd) **1** and cpd **2** were tested for hDAAO inhibition with D-serine as substrate (solid lines) and counter assay inhibition (dashed lines). Neither compound produced any inhibition in the counter assay. (B) Cpd **1** and cpd **2** inhibited hDAAO in the hDAAO inhibition assay with D-phenylglycine as substrate and using LC-MS for direct product detection. (C) Cpd **1** and cpd **2** inhibited rDAAO, albeit less potently than they inhibited hDAAO. (D) Jump-dilution assay example data for cpd **2**. In the Amplex Red platform, activity of hDAAO was monitored kinetically as production of fluorescent product over time. In the ' k_{off} ' condition (squares; '200 nM then 5 nM'), 200 nM cpd **2** (an inhibitory concentration; see Figure 2A) was rapidly diluted to 5 nM (a non-inhibitory concentration). Initially hDAAO was inhibited as reported by a shallow slope of product production defined as low initial velocity (v_i). Over time, inhibitor dissociates and a more rapid, steady-state velocity of product production (v_s) was observed. Quantitative data from each of these assays are presented in Table 1.

inhibitors [13,22,27,30,40], compound **2** displayed the kinetic properties of a canonical, active-site-bound hDAAO inhibitor.

Compound **2** bound to hDAAO in an active-site lid-open conformation

The binding mode of compound **2** to the hDAAO:FAD holoenzyme was determined by X-ray crystallography (crystallographic data in Table 2). In agreement with our kinetic observations (Figure 2), compound **2** occupied the active site of hDAAO adjacent to the FAD cofactor. The binding interaction was consistent with previously published cocrystal structures of hDAAO with small aryl carboxylic acid inhibitors or carboxylic acid bioisosteres [13,22,27,30] and included a bidentate hydrogen bond from the compound propanoate arm to the guanidinium group of Arg²⁸³ (Figure 3A). This propanoic acid-binding interaction was further stabilized by hydrogen bonds with Tyr²²⁸ and Tyr⁵⁵ (Figure 3A). The Tyr⁵⁵ interaction was only available following local rearrangement of the side chains of the active site because of inhibitor binding. This interaction with Tyr⁵⁵ was not seen in past hDAAO–ligand cocrystal structures (for example, see Figure 4B).

Additional interactions not observed in previous hDAAO–ligand structures included a hydrogen bond between the coumarin hydroxyl and the carbonyl backbone of Gln⁵³ and a water molecule interaction with the cyclic oxygen and carbonyl of compound **2**'s coumarin ring (Figure 3B).

The flexible propanoate arm allowed the coumarin portion of compound **2** to extend at 90° relative to the face of the flavin ring into the centre of the ligand-binding site. This active-site area, also termed a 'subpocket' [30], is known to associate with the bulky side chains of DAAO substrates such as D-tryptophan [28] and is occupied by portions of some DAAO inhibitors [13,30]. The hDAAO–compound **2** structure demonstrated that this subpocket is even more flexible than previously envisioned; it accommodates conformational rearrangements that allow the phenyl group on the 4 position of the coumarin ring to occupy a previously undefined pocket in hDAAO. This new hDAAO pocket was generated by the movement of amino acids 218–224, part of the active-site lid of hDAAO [28], away from the inhibitor pocket, allowing the compound **2** phenyl group to occupy space previously occupied by Tyr²²⁴ (Figure 4). The movement of Tyr²²⁴ away from the active-site pocket allowed Tyr⁵⁵ to assume a rotamer

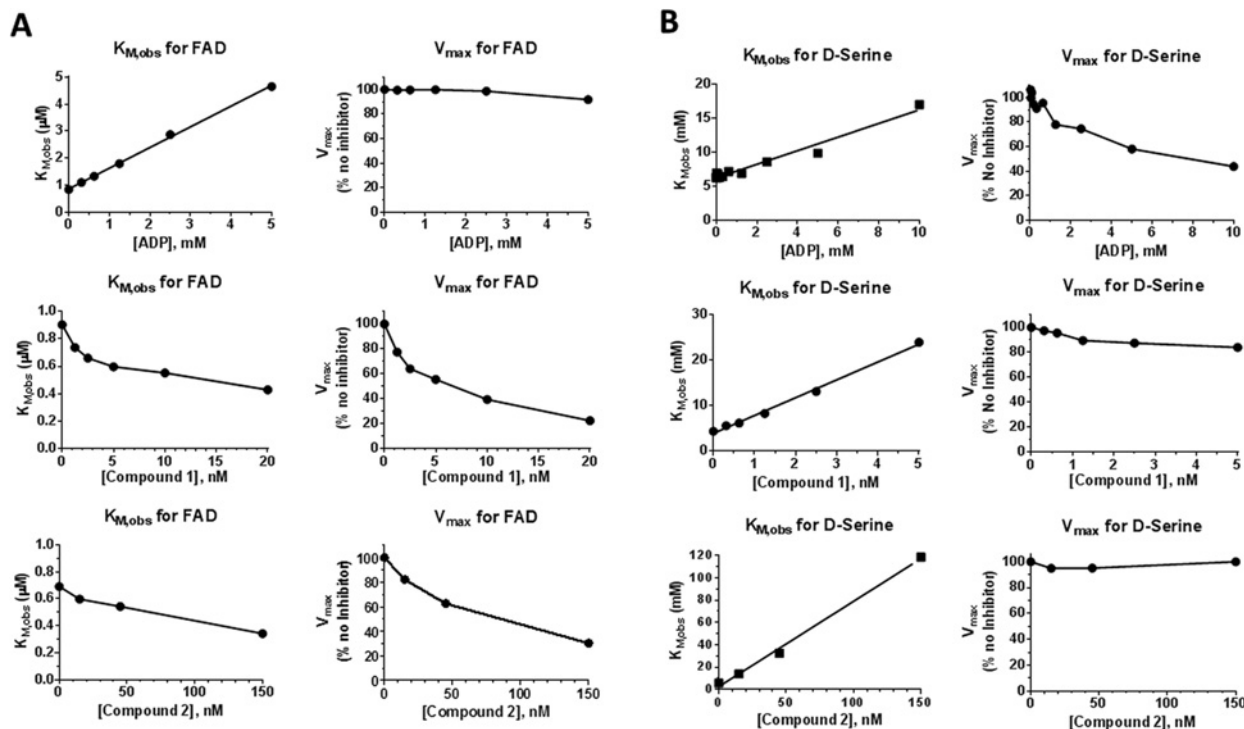


Figure 2 Determination of compound kinetic behavior in FAD- and D-serine saturation experiments

(A) Under conditions of constant, high (50 mM) D-serine concentration, FAD saturation experiments were performed. Using non-linear curve-fitting, $K_{M,obs,FAD}$ (left) and V_{max} (right) for FAD were determined at variable concentrations of tested inhibitor. (B) Reciprocally to Figure 2(A), under conditions of constant, high (40 μM) FAD concentration, D-serine saturation experiments were performed to obtain $K_{M,obs,D-ser}$ (left) and V_{max} (right) values at variable concentrations of tested inhibitor.

conformation extending into the pocket where it was stabilized by π - π -stacking interactions with the coumarin heterocycle and hydrogen-bonding interactions with Arg²⁸³.

Similar to substrates [28,29], but unlike other high-affinity hDAAO ligands [13,22,27,30], no portion of compound 2 π - π -stacked with the isoalloxazine ring of FAD. Also unlike other high-affinity hDAAO ligands, there was no suitable hydrogen-bond donor in compound 2 to interact with the carbonyl backbone of Gly³¹³ in hDAAO.

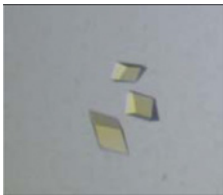
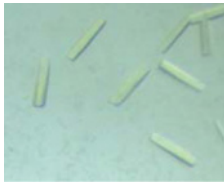
Compound 3 also bound to hDAAO in an active-site lid-open conformation

As hDAAO is a brain target relevant for schizophrenia [26], and because carboxylic acids generally restrict compounds from entering the brain [41], we sought to replace the compound 2 carboxylic acid with a bioisostere which could maintain the interaction with Arg²⁸³. After synthesizing and testing several analogues of compound 2, we discovered compound 3, in which the carboxylic acid moiety of compound 2 was replaced with a hydroxyl-pyridazinone group (structures in Table 1). Profiling of compound 3 in our panel of assays demonstrated that it was more potent than compound 2 in each of the assays, with a particular improvement in rDAAO inhibition (Table 1). In addition, it had a slow off-rate (0.015 min^{-1}), which was even slower than

the dissociation of the more potent compound 1 (0.034 min^{-1}) (Table 1). Therefore compound 3 is a relatively slow on-off compound that forms a stable, but reversible interaction with hDAAO.

The binding mode of compound 3 to the hDAAO:FAD holoenzyme was determined by X-ray crystallography. In this case, a higher resolution crystal form (P2₁2₁2₁) was identified through sparse matrix screening and the structure resolved to 2.4 Å (Table 2). Superimposition of the compound 2 and compound 3 structures [RMSD (root-mean-square deviation) = 0.543 Å (301–301 atoms)] showed an overall similar binding pose within the hDAAO active-site pocket (Figure 5A). The ketone and hydroxyl groups of compound 3 formed hydrogen bonds with Arg²⁸³ (Figure 5B), demonstrating that the hydroxyl-pyridazinone was an effective bioisosteric replacement of the carboxylic acid. The hydroxyl-pyridazinone substituent was stabilized in the hDAAO pocket by a total of five hydrogen bonds, two with Arg²⁸³, one with the Tyr²²⁸ hydroxyl, one with the Tyr⁵⁵ hydroxyl, and one with the backbone carbonyl of Gly³¹³ (Figure 5B). On the other end of the molecules, the phenyl groups of compounds 2 and 3 both occupied the same activesite lid-open space in hDAAO. In the compound 3-hDAAO structure, amino acids 219–222 were not included in the refined structure because of a lack of defined electron density. However, we defined the compound 3-hDAAO structure as active-site lid open based upon two points of evidence: (1) The phenyl group of compound 3 overlaid with the

Table 2 Crystallographic data

Crystal	hDAAO:FAD:Compound 2	hDAAO:FAD:Compound 3
PDB ID	4QFD	4QFC
Space group	P 32 2 1	P212121
Crystal morphology		
Unit cell		
<i>a</i> (Å)	86.5	44.4
<i>b</i> (Å)	86.5	60.9
<i>c</i> (Å)	188	258.5
Alpha	90	90
Beta	90	90
Gamma	120	90
Data collection		
Beamline	SSRL7-1	APS 21-idf
Resolution (Å)	2.85–19.91	2.40–43.79
Highest resolution shell	2.85–2.92	2.40–2.46
<i>R</i> _{merge}	0.069	0.096
Highest resolution shell	0.728	0.486
I/Sigma	21.8	12.25
Highest resolution shell	3.2	3.2
Completeness (%)	99.1	99.6
Highest resolution shell	99.8	99.9
Wilson B (Å ²)	69.6	40.26
Refinement		
Resolution (Å)	2.85	2.4
<i>R</i> _{work}	0.245	0.176
<i>R</i> _{free}	0.286	0.227
RMSD bonds (Å)	0.019	0.013
RMSD angles (°)	1.969	1.595

phenyl group of compound **2** and would have sterically clashed with a closed active-site lid. (2) Movement of the Tyr²²⁴ backbone and side chain of hDAAO was nearly identical in both compounds **2** and **3**-hDAAO structures (Figure 5A), confirming that at least this portion of the lid moves away from the ligand. As compound **3** is a slightly larger molecule than compound **2**, to accommodate this ligand, compound **3** had a 'tilt' through the subpocket of the active site (arrow in Figure 5A). This path through the active-site subpocket was observed in a prior crystal structure of hDAAO bound to a different ligand [SEP-137 in [13]; protein data bank (pdb) ID: 3ZNO].

Analogues of compounds **2** and **3** explore the importance of the active-site lid open conformation

To explore the importance of the active-site lid open conformation, we tested compound **4** for hDAAO inhibitory potency.

As shown in Table 1, compound **4**, which is a compound **2** analogue lacking the phenyl group that occupied the active-site lid-open pocket, was a poor hDAAO inhibitor with potency approximately 500-fold weaker than compound **2**. This result suggests that the active-site lid-open conformation facilitated binding of compound **2**. We also tested two synthetic intermediates of compound **3** (see Supplementary Figure S1; available at <http://www.bioscirep.org/bsr/034/bsr034e133add.htm>). As shown in Table 1, these two compounds, compounds **5** and **6**, displayed potency in several of our biochemical assays that was similar to the potency of compound **3** (IC₅₀ values within 5–10-fold). This result, unsurprising based upon data in the literature-testing compounds very similar to compounds **5** and **6** [30], suggests that for these hydroxyl-pyridazinone-containing compounds, the movement of the active-site lid to an open conformation did not enhance inhibitor potency.

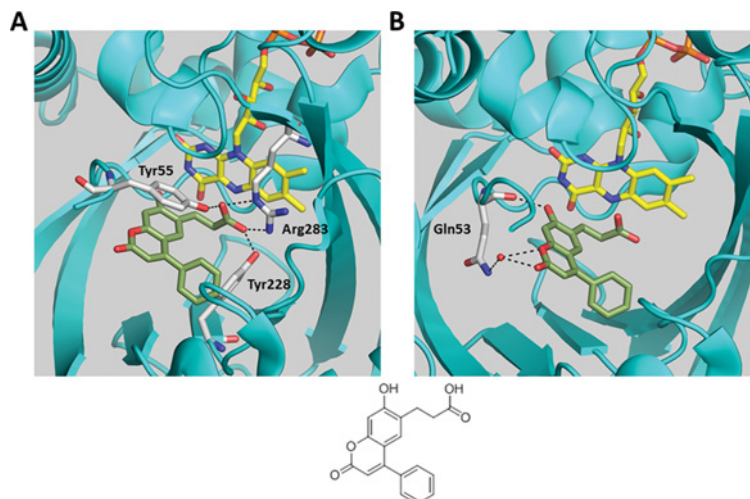


Figure 3 Cpd **2** interacts with the active site of hDAAO

In this figure and in subsequent crystallography images, illustrated amino acid side chain carbons are uncoloured, carbons of FAD are yellow, and ligand carbons are differentially coloured. Compound structures of ligands included in the crystallographic images are displayed at the bottom of the images. **(A)** In the X-ray crystal structure, cpd **2** (green) binds in the active site of hDAAO adjacent to the FAD cofactor. The carboxylic acid moiety of cpd **2** forms four different hydrogen bonds (dashed lines) with Arg²⁸³, Tyr⁵⁵ and Tyr²²⁸ of hDAAO. The aromatic ring of the Tyr⁵⁵ side chain also forms a π - π stacking interaction with the coumarin of cpd **2** (π - π stacking interactions not shown for image clarity). **(B)** Unlike other hDAAO inhibitors described in the literature, cpd **2** forms hydrogen bonds with the carbonyl backbone of hDAAO Gln⁵³ and forms a hydrogen bond with a water molecule (red sphere).

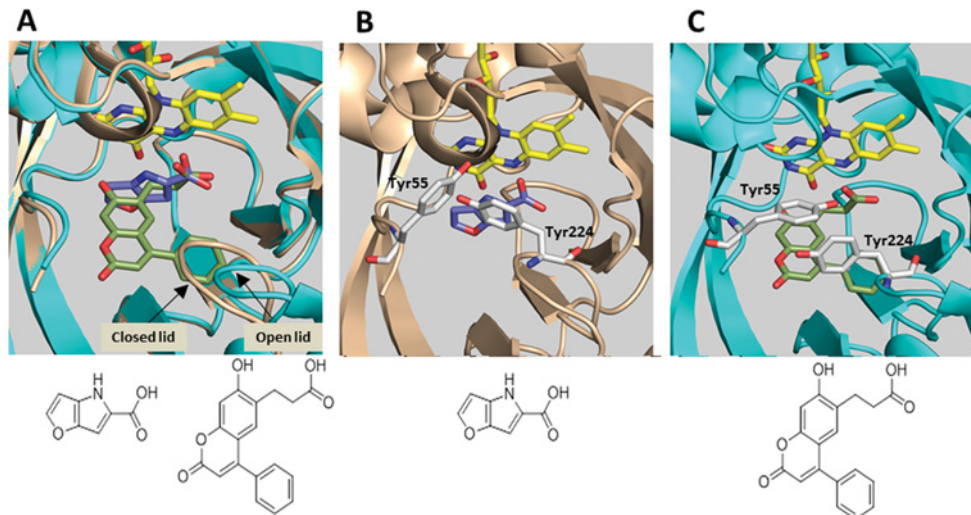


Figure 4 Cpd **2** binds to hDAAO in an active-site lid-open conformation

Overlay of the previously published (pdb ID: 3CUK [27]) cpd **1**-hDAAO structure with the cpd **2**-hDAAO structure. In all panels, the cpd **1**-hDAAO protein backbone is brown and the cpd **2**-hDAAO protein backbone is teal. Cpd **1** carbons are blue and cpd **2** carbons are green in all images. **(A)** In the overlay, the primary distinctive movement of the hDAAO backbone is the active-site lid (a loop comprised amino acids 218–224). Relative to the hDAAO–compound **1** structure, this loop moves away from the hDAAO active site when hDAAO is bound to cpd **2**. The cpd **2**-induced hDAAO conformation is defined as ‘active-site lid open,’ consistent with past publications [28]. In these panels, solvent exposure and, hence, substrate access is down and towards the viewer, just past the active-site lid. **(B)** In the active-site lid closed conformation of hDAAO with cpd **1**, Tyr²²⁴, a part of the active-site lid, is in proximity to the ligand. **(C)** In the active-site lid-open conformation of hDAAO with cpd **2**, Tyr²²⁴ moves away from the ligand, and the Tyr⁵⁵ side chain rotates towards the ligand.

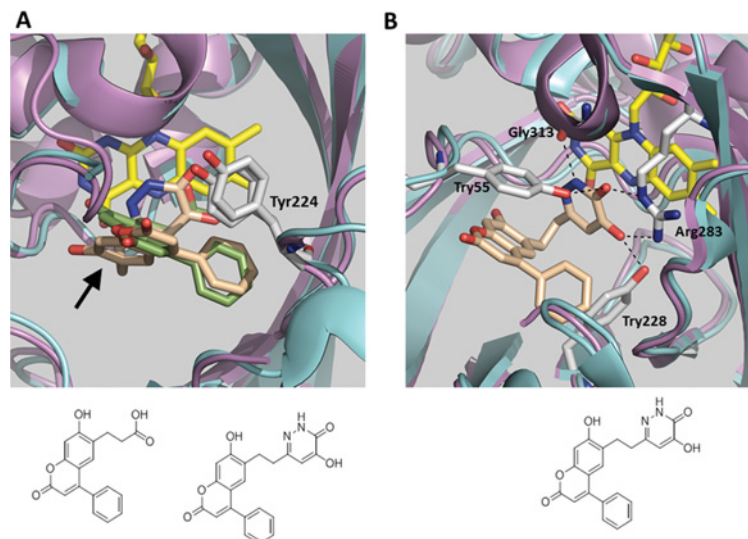


Figure 5 Cpd **3** binds to hDAAO in an active-site lid-open conformation

In these panels, the carbons of cpd **2** are green and compound **3** carbons are tan. **(A)** An overlay of the active-site structures of hDAAO in complex with cpd **2** and cpd **3**, oriented such that the viewer is looking down into the hDAAO subpocket. The hydroxyl-pyridazinone group of cpd **3** overlaps with the carboxylic acid of cpd **2**. The phenyl groups of both compounds also overlap. Relative to cpd **2**, cpd **3** has a tilted path through the hDAAO active-site subpocket (arrow). In each structure, Tyr²²⁴ and associated peptide backbone is tilted away from the active-site, consistent with the active-site lid-open conformation. **(B)** The hydroxyl-pyridazinone group of cpd **3** is an effective carboxylic acid bioisostere, forming hydrogen bonds with Tyr⁵⁵, Arg²⁸³ and Tyr²²⁸. These are the same interactions formed by the carboxylic acid moiety of cpd **2** (Figure 3A). The N on the pyridazinone ring forms a hydrogen bond with the carbonyl in the backbone of hDAAO Gly³¹³. Although not shown for clarity, the carbonyl moiety on the cpd **3** coumarin ring forms additional hydrogen bonds with a water molecule and with an N-H from the hDAAO backbone at Leu⁵⁶.

DISCUSSION

In an effort to identify novel hDAAO inhibitors, we used computational tools to identify commercially available, putative bisubstrate analogue-like compounds. We screened a library of approximately 1000 of these compounds for hDAAO inhibition. The most potent hit from that screen, compound **2**, had a structure unlike existing hDAAO inhibitors. Although our library was designed to select compounds that would be both D-serine and FAD-competitive, kinetic experiments demonstrated that compound **2** was actually FAD uncompetitive. Consistent with this observation, the ternary co-crystal structure of hDAAO with compound **2** and FAD demonstrated that compound **2** fit into the hDAAO active site adjacent to FAD. The bulky, aromatic portion of compound **2** occupied the hDAAO subpocket and stabilized an opening of the active-site lid. This finding opens the possibility of discovering structurally more diverse DAAO ligands.

Compound **2** interacts with hDAAO via several interactions that are not seen in other hDAAO inhibitors. The most striking feature is the movement of amino acids 218–224 (a portion of the active-site lid) several angstroms away from the rest of the hDAAO active site (Figure 4A). This backbone movement clears Tyr²²⁴ away from the active site. As Tyr²²⁴ is thought to act as a gatekeeper, controlling compound/substrate access to the

subpocket [13,28,30], the major backbone movement facilitates access of compound **2** to the subpocket region. An amino acid side chain movement facilitated by the Tyr²²⁴ retreat is the rotation of Tyr⁵⁵ towards compound **2**, forming π - π stacking and hydrogen bonds with compound **2**. Other novel features of the compound **2**-hDAAO structure are hydrogen bonds between the coumarin bicyclic ring of compound **2** with water and hDAAO (Figure 3B). This new structure is also interesting because of what it lacks. High-affinity hDAAO inhibitors reported by Merck [27], Pfizer [22], Johns Hopkins Brain Science Institute [40], Astellas [30], and ourselves [13] typically have two features in common: (1) a hydrogen-bond donor-oriented towards the carbonyl of hDAAO Gly³¹³, and (2) an aromatic ring that can π - π stack with the isoalloxazine ring in FAD. Although some high-affinity hDAAO inhibitors lack interaction with hDAAO Gly³¹³ (for example, compound **5** from [13]; pdb ID: 3ZNP), these compounds still are stabilized by the π - π stack with FAD. Because compound **2** is a high-potency hDAAO inhibitor ($K_i = 7$ nM) which lacks both of these two features, the novel interactions of compound **2** with hDAAO are presumably strong enough to make up for loss of these two interactions.

Guided by high-affinity ligands that contain a hydroxyl-pyridazinone group [30], we designed compound **3**. In our compound scaffold, hydroxyl-pyridazinone was an effective bioisosteric replacement for the carboxylic acid of compound **2**. Indeed, compound **3**, unlike compound **2**, displayed the two

modes of interaction with hDAAO discussed above: a hydrogen bond with Gly³¹³ of hDAAO and a π - π stacking interaction with FAD (Figure 5B). Compound **3** was approximately 2-fold more potent as a hDAAO inhibitor, with enhanced potency driven largely by a particularly slow k_{off} (Table 1). However, this rather modest potency boost after gaining two additional major hDAAO interactions suggest that the path through the subpocket by compound **3** is less favourable than for compound **2** (Figure 5A), or that some of the interactions found in compound **2** but not in compound **3** (see Figure 3B for two examples) are key drivers of binding affinity and, hence, inhibitory potency.

This study enables us to comment on the rigidity or flexibility of various regions of the hDAAO active site. In all hDAAO substrate and inhibitor complexes examined, including the compounds reported here, Arg²⁸³ and FAD appear inflexible. This rigidity could be expected as the Arg²⁸³-carboxylic acid association in substrates is critical to position the substrate in the correct orientation on the *re* face of the flavin portion of the FAD cofactor to facilitate oxidation [2]. More distant from the precise site of the oxidative reaction, the hDAAO active site appears to be more flexible. The region termed the subpocket [30] (occupied by the coumarin ring in compounds **2** and **3**), has demonstrated flexibility in past structures, particularly in rotamer movements of Tyr²²⁴ [13,28,30]. In this study, with the hDAAO backbone movement causing a several angstrom Tyr²²⁴ movement away from the active site, additional flexibility in the subpocket is revealed. This can be observed most clearly by the different routes ligands traverse through this region (e.g. Figure 5A). Finally, the active-site lid (a loop formed by amino acids 216–224) may be a region of extensive flexibility. We did not observe electron density for the full active-site lid in the compound **3**-hDAAO structure, indicating that this flexibility is associated with structural heterogeneity. Additional structural information will be required to make firm conclusions about the various conformations that can be adopted by this region of hDAAO. The flexibility/adaptability of the DAAO active site correlates well with its broad substrate specificity: the rearrangement of residue side chains located on the *re* side of the flavin isoalloxazine ring allows DAAO to bind D-amino acids with significantly different size, including unnatural ones such as cephalosporin C and naphthyl-amino acids [42,43].

The active-site lid of DAAO has long been suspected of being a mobile region of the protein, which must open to allow entry of D-amino acids into the DAAO active site [28,44]. Following substrate entry, the closed lid conformation of DAAO generates a hydrophobic environment that contributes to DAAO substrate specificity [45] and facilitates hydride transfer during substrate oxidation [28]. To date, all structures of yeast, pig, and human DAAO, whether in the substrate-bound, inhibitor-bound, or unbound forms, have portrayed DAAO with this lid closed. Thus, the structures reported here are revealing in that, by capturing hDAAO in a lid-open conformation, they provide direct evidence which confirms past hypotheses of lid flexibility [28,44]. Compounds **2** and **3** are potent hDAAO inhibitors with K_i values <10 nM and slow off-rates (for example, compound

3 has a dissociative half-life of nearly 1 h; Table 1). Thus, this ligand-induced, active-site lid-open conformation is an alternative, stable conformation of hDAAO. Although the lid-open conformation is stable, it is revealing that the non-substrate-bound form of hDAAO has only been crystalized in the closed conformation [29]. This result suggests that, although the active-site lid can sample at least two distinct conformations, the closed form is presumably a more favourable, lower free-energy state. As seen with compounds **4**, **5** and **6** (Table 1), the lid-open conformation has variable influence on inhibitor potency. In the compound **2** scaffold, loss of the phenyl group that occupies the active-site lid-open pocket greatly reduced potency and, presumably, affinity (compound **4** in Table 1). However, in the hydroxyl-pyridazinone compound series, the additional interactions afforded by the lid-open conformation did not enhance inhibitory potency (compare compound **3** with compounds **5** and **6** in Table 1). Further experiments are needed to explore the energetic favourability of the active-site lid-open versus -closed conformations of hDAAO. As a final consideration of the relevance of the active-site lid-open conformation, because compound **3** is a potent rDAAO inhibitor (Table 1), this lid-open conformation is likely to exist in DAAO proteins from non-human species as well.

Multiple groups have pursued the discovery of potent, brain-penetrant, drug-like hDAAO inhibitors for use in treating schizophrenia and other nervous system disorders [26]. Thus, the identification of a novel hDAAO conformation could guide the design of the next generation of hDAAO inhibitors. The structures described herein reveal a lid-open space for the design of DAAO inhibitors and show that π - π stacking interactions with FAD are not required for potent inhibition. As we expected, in *in vivo* studies in which compound **2** or **3** were dosed intraperitoneally in mice, each compound displayed low brain penetration (brain:plasma compound ratios <0.05; results not shown). Like all existing high-affinity hDAAO inhibitors, interaction of these compounds with Arg²⁸³ of hDAAO requires a carboxylic acid or other electronegative moiety, a feature that is known to reduce brain penetration [41]. Therefore we hypothesize that one could optimize the interaction of compound **2**-like compounds with the subpocket and newly revealed active-site lid-open pocket. Potency gained by optimizing ligand binding in these hDAAO regions could conceivably reduce the need for extensive Arg²⁸³ association, and, thus, could facilitate the creation of novel inhibitors of hDAAO.

AUTHOR CONTRIBUTION

Ryan Terry-Lorenzo managed the overall project, performed all the enzymatic experiments, and wrote the paper. Lawrence Chun performed all crystallographic experiments and participated in refining the structure, presenting results, and writing the paper. Scott Brown and Michele Heffernan designed and performed the computational algorithms and developed the screening library. Kevin Fang designed compound **3**. Michael Orsini performed the LC-MS/MS assay. Loredano Pollegioni provided protein reagents and project

direction. Larry Hardy, Kerry Spear and Tom Large participated in research design and strategy.

ACKNOWLEDGEMENTS

we thank the Chemists at Shanghai ChemPartner, Jason Xiang, Yinghua Yang and Lifeng Liu, for preparing compounds **3**, **5** and **6**. We also acknowledge Thomas E. Edwards and David Fox at Emerald Bio for structure refinement.

FUNDING

This work was supported by Sunovion Pharmaceuticals. L.P. is supported by Fondo di Ateneo per la Ricerca, University of Insubria.

REFERENCES

- Pollegioni, L. and Sacchi, S. (2010) Metabolism of the neuromodulator D-serine. *Cell. Mol. Life Sci.* **67**, 2387–2404 [CrossRef PubMed](#)
- Sacchi, S., Caldinelli, L., Cappelletti, P., Pollegioni, L. and Molla, G. (2012) Structure-function relationships in human D-amino acid oxidase. *Amino Acids* **43**, 1833–1850 [CrossRef PubMed](#)
- Konno, R., Sasaki, M., Asakura, S., Fukui, K., Enami, J. and Niwa, A. (1997) D-amino-acid oxidase is not present in the mouse liver. *Biochim. Biophys. Acta* **1335**, 173–181 [CrossRef PubMed](#)
- Konno, R., Niwa, A. and Yasumura, Y. (1990) Intestinal bacterial origin of D-alanine in urine of mutant mice lacking D-amino-acid oxidase. *Biochem. J.* **268**, 263–265 [PubMed](#)
- Hashimoto, A., Nishikawa, T., Hayashi, T., Fujii, N., Harada, K., Oka, T. and Takahashi, K. (1992) The presence of free D-serine in rat brain. *FEBS Lett.* **296**, 33–36 [CrossRef PubMed](#)
- Hashimoto, A., Oka, T. and Nishikawa, T. (1995) Extracellular concentration of endogenous free D-serine in the rat brain as revealed by *in vivo* microdialysis. *Neuroscience* **66**, 635–643 [CrossRef PubMed](#)
- Panatier, A., Theodosis, D. T., Mothet, J. P., Touquet, B., Pollegioni, L., Poulain, D. A. and Oliet, S. H. (2006) Glia-derived D-serine controls NMDA receptor activity and synaptic memory. *Cell* **125**, 775–784 [CrossRef PubMed](#)
- Henneberger, C., Papouin, T., Oliet, S. H. and Rusakov, D. A. (2010) Long-term potentiation depends on release of D-serine from astrocytes. *Nature* **463**, 232–236 [CrossRef PubMed](#)
- Papouin, T., Ladepêche, L., Ruel, J., Sacchi, S., Labasque, M., Hanini, M., Groc, L., Pollegioni, L., Mothet, J. P. and Oliet, S. H. (2012) Synaptic and extrasynaptic NMDA receptors are gated by different endogenous coagonists. *Cell* **150**, 633–646 [CrossRef PubMed](#)
- Zhou, Q. and Sheng, M. (2013) NMDA receptors in nervous system diseases. *Neuropharmacology* **74**, 69–75 [CrossRef PubMed](#)
- Wolosker, H. (2011) Serine racemase and the serine shuttle between neurons and astrocytes. *Biochim. Biophys. Acta* **1814**, 1558–1566 [CrossRef PubMed](#)
- Verrall, L., Burnet, P. W., Betts, J. F. and Harrison, P. J. (2010) The neurobiology of D-amino acid oxidase and its involvement in schizophrenia. *Mol. Psychiatry* **15**, 122–137 [CrossRef PubMed](#)
- Hopkins, S. C., Heffernan, M. L., Saraswat, L. D., Bowen, C. A., Melnick, L., Hardy, L. W., Orsini, M. A., Allen, M. S., Koch, P., Spear, K. L. et al. (2013) Structural, kinetic, and pharmacodynamic mechanisms of D-amino acid oxidase inhibition by small molecules. *J. Med. Chem.* **56**, 3710–3724 [CrossRef PubMed](#)
- Strick, C. A., Li, C., Scott, L., Harvey, B., Hajos, M., Steyn, S. J., Piotrowski, M. A., James, L. C., Downs, J. T., Rago, B. et al. (2011) Modulation of NMDA receptor function by inhibition of D-amino acid oxidase in rodent brain. *Neuropharmacology* **61**, 1001–1015 [CrossRef PubMed](#)
- Maekawa, M., Watanabe, M., Yamaguchi, S., Konno, R. and Hori, Y. (2005) Spatial learning and long-term potentiation of mutant mice lacking D-amino-acid oxidase. *Neurosci. Res.* **53**, 34–38 [CrossRef PubMed](#)
- Almond, S. L., Fradley, R. L., Armstrong, E. J., Heavens, R. B., Rutter, A. R., Newman, R. J., Chiu, C. S., Konno, R., Hutson, P. H. and Brandon, N. J. (2006) Behavioral and biochemical characterization of a mutant mouse strain lacking D-amino acid oxidase activity and its implications for schizophrenia. *Mol. Cell Neurosci.* **32**, 324–334 [CrossRef PubMed](#)
- Basu, A. C., Tsai, G. E., Ma, C. L., Ehmsen, J. T., Mustafa, A. K., Han, L., Jiang, Z. I., Benneyworth, M. A., Froimowitz, M. P., Lange, N. et al. (2009) Targeted disruption of serine racemase affects glutamatergic neurotransmission and behavior. *Mol. Psychiatry* **14**, 719–727 [CrossRef PubMed](#)
- Balu, D. T., Li, Y., Puhl, M. D., Benneyworth, M. A., Basu, A. C., Takagi, S., Bolshakov, V. Y. and Coyle, J. T. (2013) Multiple risk pathways for schizophrenia converge in serine racemase knockout mice, a mouse model of NMDA receptor hypofunction. *Proc. Natl. Acad. Sci. U. S. A.* **110**, E2400–E2409 [CrossRef PubMed](#)
- Kantrowitz, J. T. and Javitt, D. C. (2010) N-methyl-D-aspartate (NMDA) receptor dysfunction or dysregulation: the final common pathway on the road to schizophrenia? *Brain Res. Bull.* **83**, 108–121 [CrossRef PubMed](#)
- Lisman, J. E., Coyle, J. T., Green, R. W., Javitt, D. C., Benes, F. M., Heckers, S. and Grace, A. A. (2008) Circuit-based framework for understanding neurotransmitter and risk gene interactions in schizophrenia. *Trends Neurosci.* **31**, 234–242 [CrossRef PubMed](#)
- Ferraris, D., Duvall, B., Ko, Y. S., Thomas, A. G., Rojas, C., Majer, P., Hashimoto, K. and Tsukamoto, T. (2008) Synthesis and biological evaluation of D-amino acid oxidase inhibitors. *J. Med. Chem.* **51**, 3357–3359 [CrossRef PubMed](#)
- Duplantier, A. J., Becker, S. L., Bohanon, M. J., Borzilleri, K. A., Chrunk, B. A., Downs, J. T., Hu, L. Y., El-Kattan, A., James, L. C., Liu, S. et al. (2009) Discovery, SAR, and pharmacokinetics of a novel 3-hydroxyquinolin-2(1H)-one series of potent D-amino acid oxidase (DAAO) inhibitors. *J. Med. Chem.* **52**, 3576–3585 [CrossRef PubMed](#)
- Hopkins, S. C., Zhao, F. Y., Bowen, C. A., Fang, X., Wei, H., Heffernan, M. L., Spear, K. L., Spanswick, D. C., Varney, M. A. and Large, T. H. (2013) Pharmacodynamic effects of a D-amino acid oxidase inhibitor indicate a spinal site of action in rat models of neuropathic pain. *J. Pharmacol. Exp. Therap.* **345**, 502–511 [CrossRef](#)
- Zhao, W. J., Gao, Z. Y., Wei, H., Nie, H. Z., Zhao, Q., Zhou, X. J. and Wang, Y. X. (2010) Spinal D-amino acid oxidase contributes to neuropathic pain in rats. *J. Pharmacol. Exp. Therap.* **332**, 248–254 [CrossRef](#)
- Lu, J. M., Gong, N., Wang, Y. C. and Wang, Y. X. (2012) D-Amino acid oxidase-mediated increase in spinal hydrogen peroxide is mainly responsible for formalin-induced tonic pain. *Br. J. Pharmacol.* **165**, 1941–1955 [CrossRef PubMed](#)
- Sacchi, S., Rosini, E., Pollegioni, L. and Molla, G. (2013) D-amino acid oxidase inhibitors as a novel class of drugs for schizophrenia therapy. *Curr. Pharm. Des.* **19**, 2499–2511 [CrossRef PubMed](#)

- 27 Sparey, T., Abeywickrema, P., Almond, S., Brandon, N., Byrne, N., Campbell, A., Hutson, P. H., Jacobson, M., Jones, B., Munshi, S. et al. (2008) The discovery of fused pyrrole carboxylic acids as novel, potent D-amino acid oxidase (DAO) inhibitors. *Bioorg. Med. Chem. Lett.* **18**, 3386–3391 [CrossRef PubMed](#)
- 28 Todone, F., Vanoni, M. A., Mozzarelli, A., Bolognesi, M., Coda, A., Curti, B. and Mattevi, A. (1997) Active site plasticity in D-amino acid oxidase: a crystallographic analysis. *Biochemistry* **36**, 5853–5860 [CrossRef PubMed](#)
- 29 Kawazoe, T., Tsuge, H., Imagawa, T., Aki, K., Kuramitsu, S. and Fukui, K. (2007) Structural basis of D-DOPA oxidation by D-amino acid oxidase: alternative pathway for dopamine biosynthesis. *Biochem. Biophys. Res. Commun.* **355**, 385–391 [CrossRef PubMed](#)
- 30 Hondo, T., Warizaya, M., Niimi, T., Namatame, I., Yamaguchi, T., Nakanishi, K., Hamajima, T., Harada, K., Sakashita, H., Matsumoto, Y. et al. (2013) 4-Hydroxypyridazin-3(2H)-one derivatives as novel D-amino acid oxidase inhibitors. *J. Med. Chem.* **56**, 3582–3592 [CrossRef PubMed](#)
- 31 Raje, M., Hin, N., Duvall, B., Ferraris, D. V., Berry, J. F., Thomas, A. G., Alt, J., Rojas, C., Slusher, B. S. and Tsukamoto, T. (2013) Synthesis of kojic acid derivatives as secondary binding site probes of D-amino acid oxidase. *Bioorg. Med. Chem. Lett.* **23**, 3910–3913 [CrossRef PubMed](#)
- 32 Molla, G., Sacchi, S., Bernasconi, M., Pilone, M. S., Fukui, K. and Pollegioni, L. (2006) Characterization of human D-amino acid oxidase. *FEBS Lett.* **580**, 2358–2364 [CrossRef PubMed](#)
- 33 Caldinelli, L., Molla, G., Sacchi, S., Pilone, M. S. and Pollegioni, L. (2009) Relevance of weak flavin binding in human D-amino acid oxidase. *Protein Sci.* **18**, 801–810 [PubMed](#)
- 34 Yagi, K., Ozawa, T. and Nagatsu, T. (1960) Mechanism of inhibition of D-amino acid oxidase. IV. Inhibitory action of chlorpromazine. *Biochim. Biophys. Acta* **43**, 310–317 [CrossRef PubMed](#)
- 35 Sacchi, S., Bernasconi, M., Martineau, M., Mothet, J. P., Ruzzene, M., Pilone, M. S., Pollegioni, L. and Molla, G. (2008) pLG72 modulates intracellular D-serine levels through its interaction with D-amino acid oxidase: effect on schizophrenia susceptibility. *J. Biol. Chem.* **283**, 22244–22256 [CrossRef PubMed](#)
- 36 Brandish, P. E., Chiu, C. S., Schneeweis, J., Brandon, N. J., Leech, C. L., Kornienko, O., Scolnick, E. M., Strulovici, B. and Zheng, W. (2006) A cell-based ultra-high-throughput screening assay for identifying inhibitors of D-amino acid oxidase. *J. Biomol. Screen* **11**, 481–487 [CrossRef PubMed](#)
- 37 Frattini, L. F., Piubelli, L., Sacchi, S., Molla, G. and Pollegioni, L. (2011) Is rat an appropriate animal model to study the involvement of D-serine catabolism in schizophrenia? Insights from characterization of D-amino acid oxidase. *FEBS J.* **278**, 4362–4373 [CrossRef PubMed](#)
- 38 Copeland, R. A., Basavapathruni, A., Moyer, M. and Scott, M. P. (2011) Impact of enzyme concentration and residence time on apparent activity recovery in jump dilution analysis. *Anal. Biochem.* **416**, 206–210 [CrossRef PubMed](#)
- 39 Kawazoe, T., Tsuge, H., Pilone, M. S. and Fukui, K. (2006) Crystal structure of human D-amino acid oxidase: context-dependent variability of the backbone conformation of the VAAGL hydrophobic stretch located at the Si-face of the flavin ring. *Protein Sci.* **15**, 2708–2717 [CrossRef PubMed](#)
- 40 Berry, J. F., Ferraris, D. V., Duvall, B., Hin, N., Rais, R., Alt, J., Thomas, A. G., Rojas, C., Hashimoto, K., Slusher, B. S. and Tsukamoto, T. (2012) Synthesis and SAR of 1-hydroxy-1H-benzodimidazole-2(3H)-ones as inhibitors of D-amino acid oxidase. *ACS Med. Chem. Lett.* **3**, 839–843 [CrossRef PubMed](#)
- 41 Di, L., Rong, H. and Feng, B. (2013) Demystifying brain penetration in central nervous system drug discovery. *Miniperspective. J. Med. Chem.* **56**, 2–12 [CrossRef](#)
- 42 Pollegioni, L., Caldinelli, L., Molla, G., Sacchi, S. and Pilone, M. S. (2004) Catalytic properties of D-amino acid oxidase in cephalosporin C bioconversion: a comparison between proteins from different sources. *Biotechnol. Prog.* **20**, 467–473 [CrossRef PubMed](#)
- 43 Caligiuri, A., D'Arrigo, E., Rosini, E., Tessaro, D., Molla, G., Servi, S. and Pollegioni, L. (2006) Enzymatic conversion of unnatural amino acids by yeast D-amino acid oxidase. *Adv. Synth. Catal.* **348**, 2183–2190 [CrossRef](#)
- 44 Mattevi, A., Vanoni, M. A., Todone, F., Rizzi, M., Teplyakov, A., Coda, A., Bolognesi, M. and Curti, B. (1996) Crystal structure of D-amino acid oxidase: a case of active site mirror-image convergent evolution with flavocytochrome b₂. *Proc. Natl. Acad. Sci. U. S. A.* **93**, 7496–7501 [CrossRef PubMed](#)
- 45 Setoyama, C., Nishina, Y., Mizutani, H., Miyahara, I., Hirotsu, K., Kamiya, N., Shiga, K. and Miura, R. (2006) Engineering the substrate specificity of porcine kidney D-amino acid oxidase by mutagenesis of the 'active-site lid'. *J. Biochem.* **139**, 873–879 [CrossRef PubMed](#)

Received 30 April 2014/10 June 2014; accepted 1 July 2014

Published as Immediate Publication 8 July 2014, doi 10.1042/BSR20140071



OPEN ACCESS

SUPPLEMENTARY DATA

Novel human D-amino acid oxidase inhibitors stabilize an active-site lid-open conformation

Ryan T. TERRY-LORENZO*¹, Lawrence E. CHUN†, Scott P. BROWN*, Michele L. R. HEFFERNAN*, Q. Kevin FANG*, Michael A. ORSINI*, Loredano POLLEGIONI‡§, Larry W. HARDY*, Kerry L. SPEAR* and Thomas H. LARGE*

*Discovery Research Department, Sunovion Pharmaceuticals, Marlborough, MA 01752, U.S.A.

†Emerald Bio, Bainbridge Island, WA 98110, U.S.A.

‡Dipartimento di Biotecnologie e Scienze della Vita, Università degli Studi dell'Insubria, Via J. H. Dunant 3, 21100 Varese, Italy

§The Protein Factory, Politecnico di Milano, ICRM-CNR Milano and Università degli Studi dell'Insubria, Via Mancinelli 7, 20131 Milano, Italy

EXPERIMENTAL

Designing the focused library

To prepare a library of compounds for screening we first filtered the then current (as of June, 2012) snapshot of the eMolecules database of commercially available compounds (<http://www.emolecules.com>; released March, 2012, and last accessed 22 January 2014). A set of molecular property filters (Table S1) were then applied to the eMolecules compounds (initially over 6 million compounds in total). This filtering reduced the total number of compounds to just over 320 000. This filtered set of eMolecules compounds was then used as input into three different computational methods: a 2D ligand-based method; a 3D ligand-based method; and a 3D structure-based method.

The ligand-based methods required a set of known active molecules. These were obtained directly from the protein–ligand structures listed in Table S2. This set of three compounds (the ‘query’ set) was used in all of the ligand-based searching on the filtered eMolecules’ compounds (the ‘database’ set). The three query compounds shown in Table S2 were selected from the set of known DAAO actives by optimization of structural diversity (i.e. dissimilarity) using ECFP-6 (extended connectivity fingerprints of length 6) [1].

Before performing the 3D calculations it was necessary to generate 3D conformations for each molecule in both query and database sets. Omega (v2.4.6) [2] was used to generate plausible sets of conformations for each database molecule using the default settings for all command-line parameters, with the exception of the following: an energy window value of 50; a maximum number of conformers of 1000; and root-mean-square conformer-clustering threshold of 0.75 Å. For the query compounds, Omega was used with default settings for everything except the maximum number of conformers, which was set to 1.

To incorporate 3D structural information into our assessment of the database compounds, we used a docking and scoring approach. There were two primary reasons for introducing protein

Table S1 Property cut-off values used to perform a first-pass triage of the full set of eMolecules compounds

All properties were calculated and filtered using Pipeline Pilot (v8.5.0.200) (Accelrys, <http://www.accelrys.com>; accessed 22 January 2014)

Property	Min	Max
Molecular mass	250	450
Hydrogen-bond donors	0	8
Hydrogen-bond acceptors	0	4
AlogP	− 0.5	4.5
Polar surface area	0	100
Rotatable bonds	0	8
Number of aromatic rings	0	4

structure into the calculation: First, we were looking to bias our screening library for active-site similarity to obtain compounds more generally compatible with the full size and shape of the DAAO active site. Secondly, we sought to explore new regions of the binding site by requiring additional positional constraints on the docked poses during the docking procedure.

In the following sections, we describe three different methods used to search the database compounds. In the final section, we describe the steps to combine the individual methods and produce the final prioritized list of candidate compounds for consideration in the screening library.

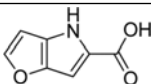
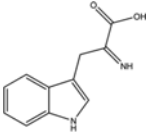
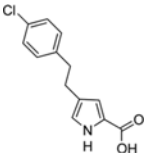
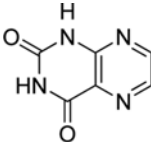
2D ligand-based calculations

To assess 2D ligand similarity against the query compounds, we used ECFP-6, which was calculated and processed within Pipeline Pilot (v8.5.0.200) with a bit length of 4096. The output from this was three separate rank-ordered lists of database compounds, one for each of the three query molecules. The compounds in each of these lists contain an ECFP-6 Tanimoto similarity value to each known active, the values of which ranged from 1.0 (identical) to 0.0 (orthogonal).

¹ To whom correspondence should be addressed (email Ryan.Terry-Lorenzo@sunovion.com).

Table S2 Chemical structures for the three query compounds used in the ligand-based strategies, along with the accompanying truncated FAD fragment

Also listed in the table are the pdb sources of the 3D coordinates for each molecule.

Identifier	Structure	Source
Compound S-1		PDB: 3CUK
Compound S-2		PDB: 1DD0
Compound S-3		PDB: 3ZNO
FAD fragment		(3D coordinates taken from each of the above structures)

3D ligand-based calculations

The three queries shown in Table S2, along with their accompanying FAD fragments, were used to perform the 3D similarity comparisons. To compare 3D similarity we used the program ROCS (v3.1.2) [3]. The ROCS calculation returns shape Tanimoto and colour Tanimoto values for the single best conformer overlay of each database molecule onto each of the three query molecules. The full calculation also incorporates an accompanying FAD fragment that adds its shape and colour to each query molecule. The 3D coordinates for each FAD fragment were obtained from the cognate structure of each query molecule (specified in Table S2). From this step we generated a separate list of rank-ordered compounds for each query, which was sorted by the combined score of shape Tanimoto plus colour Tanimoto.

3D structure-based calculations

We used the protein coordinates from the three X-ray crystallographic structures (the cognate structures for each query) listed in Table S2. To prepare the protein structures for consistent handling in the scoring procedure, we added explicit hydrogen atoms to each complex using OpenEye Scientific Software's hydrogen-atom placement algorithm in OEChem (<http://www.eyesopen.com/>; last accessed 22 January 2014). All of the database compounds were then docked into each protein structure using FRED (v2.2.5) [4]. FRED broke down the process into three phases: (1) a grid was constructed that encompassed the region of the protein within which we wished to search; (2) the input conformations for each molecule were systematically translated and rotated on the protein active-site grid to produce an exhaustive set of putative binding poses, which were then triaged down to a manageable number by initial scoring; and (3), the top-

scoring poses from (2) were passed into final score optimization to produce a single highest-scoring best pose for each compound.

To generate the grids in (1) we used the position of the crystal structure ligand to centre each grid 'box,' after which 4.0 Å was added to each side of the grid box. We added to each grid an additional pose filter that contained three constraints in the active site. The first two constraints placed two spheres with a radius 1.5 Å on FAD fragment atoms O2 and O4. The final constraint placed a 1.5 Å sphere on the atom labelled CZ in the protein active-site arginine residue (residue Arg²⁸³ in 2DU8). Any docked poses that could not place at least 1 atom of the correct functional group into each of these spheres was eliminated from consideration. Poses that survived these constraints were then scored in step (2) using CGO (Chemical Gaussian Overlay), which filtered out all but the top scoring 100 poses. The CGO score was chosen in order to provide a measure of similarity against the known ligands, which allowed for incorporation of additional bias towards experimental data. These poses were then optimized using ChemGauss3 [4] in step (3) of the docking. The above docking procedure produced three rank-ordered lists, one for each structure used.

Combining scores

To combine the information from all of the above methods we used a general framework based on Belief Theory [5] to provide a final net cumulative score. This requires all of the similarities from the ligand-based methods [6], as well as the docking scores from the structure-based method, to be converted into probabilities [7]. The individual probabilities, or 'beliefs,' from the each method were then combined in a formal way to create a total belief in the activity of each database molecule. We used equation (S1) to combine the probabilities for the ligand-based beliefs

from ECFP-6 and ROCS, and the structure-based beliefs from FRED: (S1)

$$\text{Cumulative belief} = 1 - \prod_{i=1, j=1}^{N, M} (1 - P_{i, j}) \quad (\text{S1})$$

where N is the number of methods, M is the number of queries, and $P_{i, j}$ is the probability for the i th measure on the j th query. The cumulative beliefs produced by the conjunctive combination in equation (S1) were then used to produce a final ranked list of database compounds. The top several thousand compounds from this list were retained and passed for final evaluation by a project-team medicinal chemist, who then generated the final list of compounds to be screened.

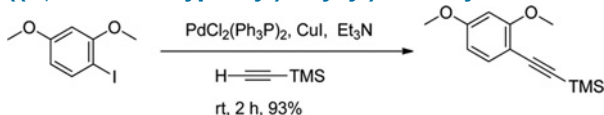
Compound screening

The focused library of 1016 compounds was screened for hDAAO inhibition using the Amplex Red-based platform. Compounds were screened at 50 and 5 μM in parallel in the hDAAO inhibition and counter assays. Hits were considered compounds in which the % inhibition at 50 μM was >35 percentage points higher in the hDAAO inhibition versus the counter assay. These hits were further characterized by determining an hDAAO IC_{50} . To quantitatively determine assay performance, a Z' factor [8] was determined using standard protocols and equations. Briefly, hDAAO activity (based upon fluorescent product produced) was determined in 32 interleaved wells each of 3 conditions: DMSO-treated (Signal), 3.3 nM compound **1**-treated (Mid value), and 3.3 μM compound **1**-treated (background). The compound **1** concentration in the Mid value condition was chosen as an approximate IC_{50} , and the background concentration was a compound **1** concentration that produced 100 % hDAAO inhibition. This experiment was repeated using three plates each on three different days. The signal and background wells were used to determine a Z' Factor, a single metric that quantitatively defines the suitability of an assay for screening by accounting for assay signal, background and S.D. of both signal and background [8].

Synthesis of compound 3

The general synthetic scheme for compound **3** is described in Supplementary Figure S1. More details are below.

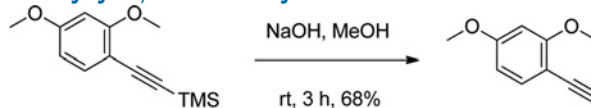
((2,4-dimethoxyphenyl)ethynyl)trimethylsilane



To a solution of 1-iodo-2,4-dimethoxybenzene (1.32 g, 5.0 mmol), $\text{PdCl}_2(\text{PPh}_3)_2$ (0.07 g, 0.1 mmol) and CuI (0.02 g, 0.1 mmol) in TEA (triethanolamine) (20 ml) (stirring for 5 min beforehand), 6.0 mmol of trimethylsilyl acetylene (0.588 g, 6.0 mmol) in 5 ml of TEA was added dropwise over 10 min under Ar atmosphere. Then the mixture was stirred at room temperature for 1.5 h. The resulting solution was filtered,

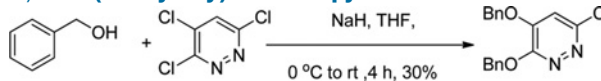
washed with brine and extracted with ethyl acetate (2×10 ml). The combined organics were dried (MgSO_4) and concentrated under vacuum to provide the crude product. Purification by flash chromatography to provide 1.1 g (93 % yield) of ((2,4-dimethoxyphenyl)ethynyl)trimethylsilane as a brown solid. ^1H NMR (400 MHz, CDCl_3) δ 7.32 (d, $J = 8.0$ Hz, 1H), 6.36 (d, $J = 8.0$ Hz, 1H), 6.34 (s, 1H), 3.78 (s, 3H), 3.72 (s, 3H), 0.25 (s, 9H). MS (ESI) m/z 235 ($\text{M} + \text{H}$)⁺.

1-Ethynyl-2,4-dimethoxybenzene



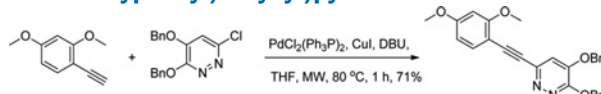
A solution of NaOH (1.60 g, 40.0 mmol) in 15 ml of water was added dropwise to [(2,4-dimethoxyphenyl)ethynyl]trimethylsilane (2.34 g, 10 mmol) in 45 ml of 50 % of CH_3OH /diethyl ether. The reaction mixture was stirred for 3 h at 25 °C. CH_3OH was removed under vacuum. The reaction mixture was diluted with ether and neutralized with 2 M HCl. The ether layer was washed with water, dried (Na_2SO_4), filtered, and the solvent removed under vacuum. Purification by flash chromatography to provide 1.1 g (68 % yield) of 1-ethynyl-2,4-dimethoxybenzene as a clear oil. ^1H NMR (400 MHz, CDCl_3) δ 7.36 (d, $J = 8.4$ Hz, 1H), 6.42 (d, $J = 8.4$ Hz, 1H), 6.41 (s, 1H), 3.84 (s, 3H), 3.78 (s, 3H), 3.25 (s, 1H). MS (ESI) m/z 163 ($\text{M} + \text{H}$)⁺.

3,4-Bis(benzyloxy)-6-chloropyridazine



To a solution of sodium hydride (4.98 g, 124.4 mmol) in THF (200 ml) was added phenylmethanol (13.45 g, 124.4 mmol) at room temperature. The resulting mixture was stirred for 1 h and then cooled to 0 °C. 3,4,6-trichloropyridazine (11.41 g, 62.2 mmol) in THF (tetrahydrofolate) (50 ml) was then added dropwise. The reaction mixture was stirred at room temperature for 4 h. EtOAc (400 ml) was added to the reaction vessel and the resulting biphasic mixture was transferred to a separator funnel. The layers were separated and the organic phase was washed with saturated aqueous NaCl (1×75 ml). The combined organics were dried (Na_2SO_4), filtered and concentrated *in vacuo*. The resulting oil was purified by flash column chromatography with 20/1 PE/EA to provide 6.2 g (30.5 % yield) of 3,4-bis(benzyloxy)-6-chloropyridazine as a white solid. MS (ESI) m/z 327.0 ($\text{M} + \text{H}$)⁺.

3,4-Bis(benzyloxy)-6-((2,4-dimethoxyphenyl)ethynyl)pyridazine



To a solution of 1-ethynyl-2,4-dimethoxybenzene (0.16 g, 1 mmol) in THF (5 ml) was added 3,4-bis(benzyloxy)-6-chloropyridazine (327 mg, 1 mmol) followed by copper iodide (0.02 g, 0.1 mmol), DBU (0.46 g, 3 mmol) and $\text{PdCl}_2(\text{Ph}_3\text{P})_2$

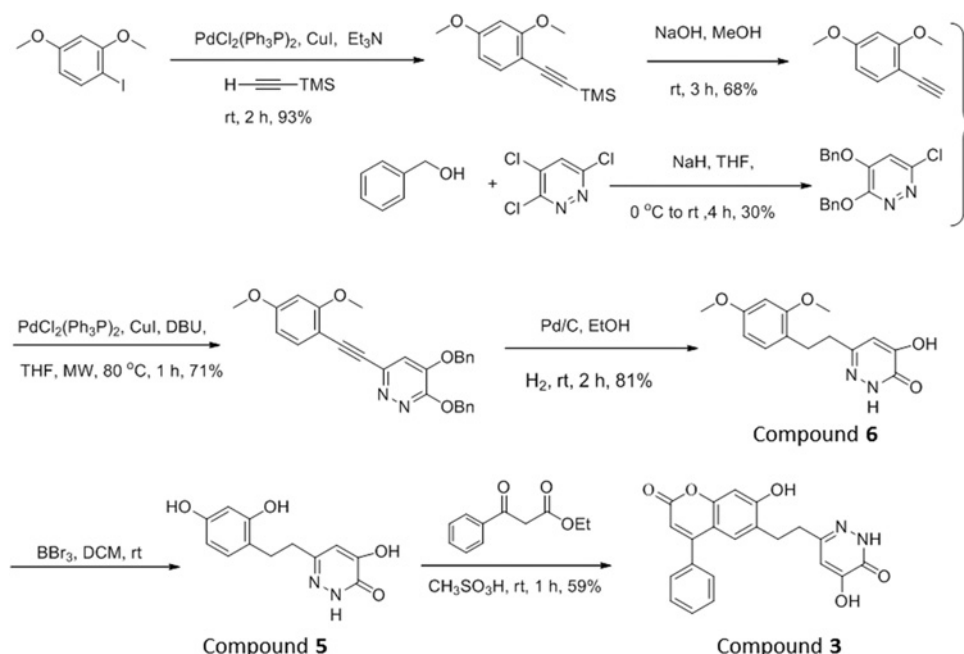
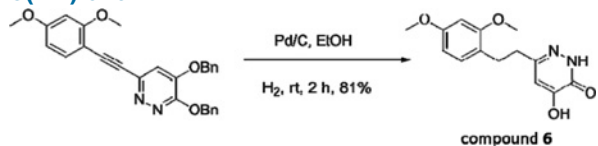


Figure S1 Chemical synthesis scheme for compound 3

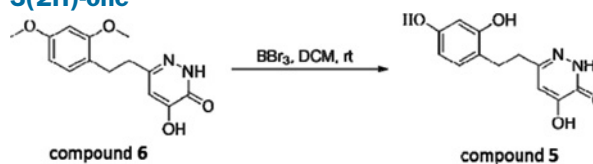
(0.04 g, 0.05 mmol) in a 20 ml microwave vial. The mixture was purged with nitrogen before the whole mixture was subjected to microwave radiation for 1 h at 85 °C. The reaction mixture was cooled to room temperature and diluted with ethyl acetate and purified by silica gel chromatography to provide 320 mg (71% yield) of 3,4-bis(benzyloxy)-6-((2,4-dimethoxyphenyl)ethynyl)pyridazine as an orange oil. MS (ESI) m/z 453 (M + H)⁺.

6-(2,4-Dimethoxyphenethyl)-4-hydroxypyridazin-3(2H)-one



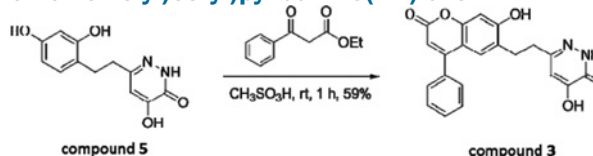
To a solution of 3,4-bis(benzyloxy)-6-((2,4-dimethoxyphenyl)ethynyl)pyridazine (**1-7**) (230 mg, 0.05 mmol) in ethanol (10 ml) under nitrogen was added palladium (10 wt.% on activated carbon, 23 mg). The reaction mixture was deoxygenated under vacuum and then hydrogenated at room temperature for 2 h. After the reaction completed, the reaction mixture was filtered through a pad of celite and washed with ethanol (2 × 25 ml). The filtrate was concentrated to provide 114 mg (81% yield) of 6-(2,4-dimethoxyphenethyl)pyridazine-3,4-diol as a brown solid. This crude product was used for the next step without further purification. ¹H NMR (400 MHz, DMSO) δ 12.64 (s, 1H), 10.69 (s, 1H), 6.99 (d, J = 8.3 Hz, 1H), 6.56–6.49 (m, 2H), 6.41 (dd, J = 8.3, 2.4 Hz, 1H), 3.75 (s, 3H), 3.72 (s, 3H), 2.77–2.71 (m, 2H), 2.68–2.61 (m, 2H). MS (ESI) m/z 277 (M + H)⁺.

6-(2,4-Dihydroxyphenethyl)-4-hydroxypyridazin-3(2H)-one



To a solution of a 6-(2,4-dimethoxyphenethyl)-4-hydroxypyridazin-3(2H)-one (2 mmol) in dry CH₂Cl₂ (5 ml) was added dropwise BBr₃ (1.2 mmol, 0.3 ml) at –20 °C. Then the reaction mixture was warmed to room temperature and stirred at that temperature overnight. HCl in methanol (1 M, 2 ml) was added to quench the reaction at 0 °C. The mixture was concentrated under vacuum. The crude product was enough pure for the use of next step. ¹H NMR (400 MHz, DMSO) δ 12.64 (s, 1H), 10.67 (s, 1H), 8.85–9.25 (m, 2H), 6.77 (d, J = 8.2 Hz, 1H), 6.51 (s, 1H), 6.26 (d, J = 2.3 Hz, 1H), 6.10 (dd, J = 8.1, 2.4 Hz, 1H), 2.70–2.60 (m, 4H), 2.54 (s, 1H). MS (ESI) m/z 249 (M + H)⁺.

4-Hydroxy-6-(2-(7-hydroxy-2-oxo-4-phenyl-2H-chromen-6-yl)ethyl)pyridazin-3(2H)-one



To a solution of 6-(2,4-dihydroxyphenethyl)-4-hydroxypyridazin-3(2H)-one (302 mg, 1.21 mmol) in methanesulfonic acid (5 ml) was added ethyl 3-oxo-3-phenylpropanoate (230 mg,

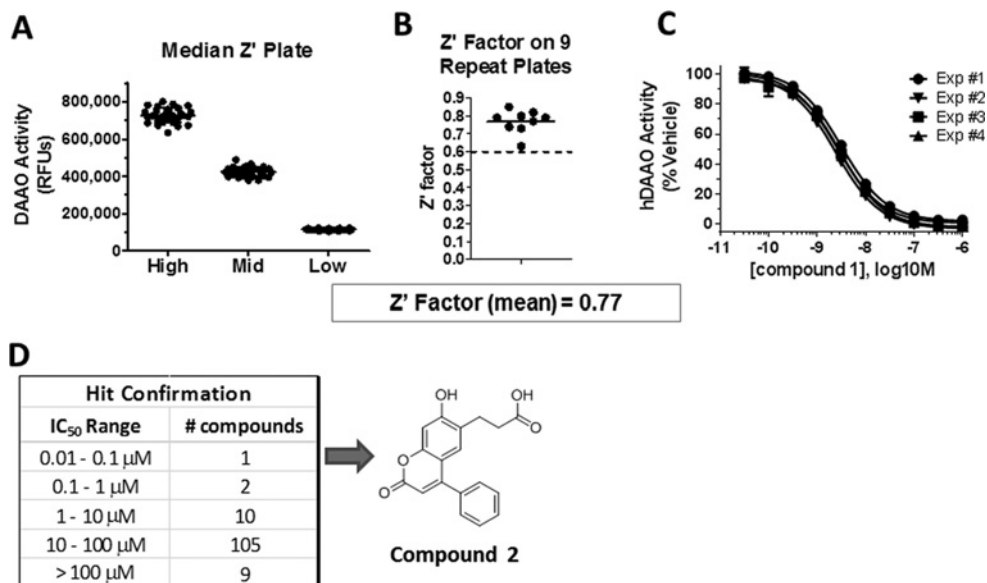


Figure S2 Screening strategy identified compound 2

(A) In the Amplex Red system in 96-well plate format, hDAAO activity, based upon RFUs (relative fluorescent units) of product produced, was determined in 32 interleaved wells each of three conditions: DMSO-treated ('High'), 3.3 nM compound 1-treated ('Mid'), and 3.3 μM compound 1-treated ('Low'). Shown in Figure 1(A) are results without normalization or background-subtraction from an average (median) plate. (B) On nine repeat plates (three plates each on three different days) of the experiment described in Figure 1A, the High and Low wells were used to determine a Z' Factor [8]. The Z' Factors on all nine plates were above 0.6, indicating that the assay was suitable for differentiating hDAAO inhibitors and non-inhibitors when screening compounds in single-dose format. (C) Inhibition curves with compound 1 in four independent experiments demonstrated assay reproducibility in reporting IC₅₀ values. (D) 127 hits from the screen were tested for hDAAO inhibitory potency. Shown are the numbers of compounds in each histogram bin of inhibitory potency. Compound 2 was the most potent hit from the screen.

1.21 mmol). The reaction mixture was stirred at room temperature for 1 h. Water (50 ml) was added to the reaction vessel and the resulting solid was collected by filtration. The solid was purified by Pre-HPLC to provide 270 mg (59% yield) of 4-hydroxy-6-(2-(7-hydroxy-2-oxo-4-phenyl-2H-chromen-6-yl)ethyl)pyridazin-3(2H)-one (compound 3) as a white solid. ¹H NMR (400 MHz, DMSO) δ 12.65 (s, 1H), 10.77 (s, 2H), 7.58–7.48 (m, 3H), 7.34 (dd, *J* = 6.4, 2.8 Hz, 2H), 6.94 (s, 1H), 6.84 (s, 1H), 6.52 (s, 1H), 6.10 (s, 1H), 2.79 (t, *J* = 6.9 Hz, 2H), 2.65 (t, *J* = 7.0 Hz, 2H). MS (ESI) *m/z* 377 (M + H)⁺.

RESULTS

Identification of compound 2 as a novel inhibitor of hDAAO

To identify the novel inhibitors of hDAAO, we performed a series of modelling techniques to guide the purchase of commercially available compounds. These techniques ultimately produced a group of compounds modelled as bisubstrate analogues containing, in a single molecule, structural features of an active site hDAAO inhibitor adjacent to structural elements of the FAD cofactor. 1016 compounds were purchased and screened for hDAAO inhibition.

To screen these molecules for hDAAO inhibition, we used an Amplex Red-based fluorescence enzyme assay to measure the hydrogen peroxide produced during the hDAAO catalytic cycle of FAD reduction and re-oxidation [9]. The assay was robust with low S.D. and good signal-to-noise ratio, as evidenced by high Z' factor [8] values (Supplementary Figures S2A and S2B). hDAAO activity was inhibited potently and reproducibly by a known hDAAO inhibitor [10,11], compound 1 (Supplementary Figure S2C and Table 2). The screen of 1016 compounds was executed, using a counter assay to exclude compounds that interfered with the HRP/hydrogen peroxide detection system. For hit confirmation, 127 compounds that displayed >35% specific hDAAO inhibition at 50 μM were characterized in concentration–response experiments to generate IC₅₀ values. The range of IC₅₀ results are listed in Supplementary Figure S2(D). The most potent hit compound was compound 2.

REFERENCES

- Rogers, D. and Hahn, M. (2010) Extended-connectivity fingerprints. *J. Chem. Inf. Model.* **50**, 742–754 [CrossRef PubMed](#)



- 2 Bostrom, J., Greenwood, J. R. and Gottfries, J. (2003) Assessing the performance of OMEGA with respect to retrieving bioactive conformations. *J. Mol. Graph Model.* **21**, 449–462 [CrossRef PubMed](#)
- 3 Grant, J. A., Gallardo, M. A. and Pickup, B. T. (1996) A fast method of molecular shape comparison: a simple application of a Gaussian description of molecular shape. *J. Comput. Chem.* **17**, 1653–1666 [CrossRef](#)
- 4 McGann, M. (2011) FRED pose prediction and virtual screening accuracy. *J. Chem. Inf. Model.* **51**, 578–596 [CrossRef PubMed](#)
- 5 Shafer, G. (1976) *A Mathematical Theory of Evidence*, Princeton University Press
- 6 Muchmore, S. W., Debe, D. A., Metz, J. T., Brown, S. P., Martin, Y. C. and Hajduk, P. J. (2008) Application of belief theory to similarity data fusion for use in analog searching and lead hopping. *J. Chem. Inf. Model.* **48**, 941–948 [CrossRef PubMed](#)
- 7 Swann, S. L., Brown, S. P., Muchmore, S. W., Patel, H., Merta, P., Locklear, J. and Hajduk, P. J. (2011) A unified, probabilistic framework for structure- and ligand-based virtual screening. *J. Med. Chem.* **54**, 1223–1232 [CrossRef PubMed](#)
- 8 Zhang, J. H., Chung, T. D. and Oldenburg, K. R. (1999) A simple statistical parameter for use in evaluation and validation of high throughput screening assays. *J. Biomol. Screen.* **4**, 67–73 [CrossRef PubMed](#)
- 9 Brandish, P. E., Chiu, C. S., Schneeweis, J., Brandon, N. J., Leech, C. L., Kornienko, O., Scolnick, E. M., Strulovici, B. and Zheng, W. (2006) A cell-based ultra-high-throughput screening assay for identifying inhibitors of D-amino acid oxidase. *J. Biomol. Screen.* **11**, 481–487 [CrossRef PubMed](#)
- 10 Sparey, T., Abeywickrema, P., Almond, S., Brandon, N., Byrne, N., Campbell, A., Hutson, P. H., Jacobson, M., Jones, B. and Munshi, S. (2008) The discovery of fused pyrrole carboxylic acids as novel, potent D-amino acid oxidase (DAO) inhibitors. *Bioorg. Med. Chem. Lett.* **18**, 3386–3391 [CrossRef PubMed](#)
- 11 Duplantier, A. J., Becker, S. L., Bohanon, M. J., Borzilleri, K. A., Chrnyk, B. A., Downs, J. T., Hu, L. Y., El-Kattan, A., James, L. C., Liu, S. et al. (2009) Discovery, SAR, and pharmacokinetics of a novel 3-hydroxyquinolin-2(1H)-one series of potent D-amino acid oxidase (DAAO) inhibitors. *J. Med. Chem.* **52**, 3576–3585 [CrossRef PubMed](#)

Received 30 April 2014/10 June 2014; accepted 1 July 2014

Published as Immediate Publication 8 July 2014, doi 10.1042/BSR20140071
